# EPR Spectrum of Fe³⁺ in Synthetic Brown Quartz

L. M. MATARRESE, J. S. WELLS, AND R. L. PETERSON

*National Bureau of Standards, Boulder, Colorado 80302*

(Received 8 March 1968)

A detailed description is given of the EPR spectrum of $Fe^{3+}$ in synthetic brown quartz (the so-called $I$ center, presumed to be interstitial). There are three equally populated sites differing only in the orientation of their principal axes, which coincide with the three twofold axes of quartz. The values of the Hamiltonian parameters that fit the data best are: $g = 2.0039$, $C_{20}(\equiv D) = 734.3G$, $C_{22}[\equiv (6^{1/2}/2)|E|] = 401.7G$, $C_{40} = 2.52G$, $C_{44} = 1.40G$, where the $C_{lm}$ are the coefficients of the Racah operators in the Hamiltonian. Lobes of the $V_{22}$, $V_{43}$, and $V_{44}$ parts of the crystal-field potential point 0.7°, 29.5°, and 26.8°, respectively, from the optic axis of quartz. The occurrence of irregular off-axis extrema of the line positions when the magnetic field is directed in the vicinity of the optic axis precludes the assignment of magnetic axes of the paramagnetic center in the usual way. All features of the spectrum are predicted accurately by computer calculations based on the derived Hamiltonian. Although the data are not conclusive evidence, they are believed to be more consistent with an assignment of the $I$ center to a substitutional site.

## I. INTRODUCTION

Our story begins with natural amethyst, a purple-colored quartz. Several years ago we began an investigation of the rich and bewildering EPR spectrum yielded by an amethyst crystal taken from a mineral collection. Suspecting that $Fe^{3+}$ was the impurity responsible for the spectrum, we interrupted its study to examine the EPR spectrum of $Fe^{3+}$ introduced into synthetic quartz crystals during growth. In these crystals, which are variously green and brown in color, we found an obvious $Fe^{3+}$ spectrum that was quite different from the dominant EPR spectrum characteristic of amethyst, although traces of the latter could be found in some of the synthetic crystals. Our preliminary report[1] on this new spectrum attributed it to substitutional $Fe^{3+}$ in three differently oriented but otherwise equivalent sites. This paper is a precise description of this spectrum. The paper directly following in this issue[2] supplements this

description with a report of our zero-field experiments on the same specimen. Details of the mathematical analysis of the spectrum have been published separately.[3]

The EPR spectrum of natural amethyst (NA) is indeed due to $Fe^{3+}$ and has been well characterized by Hutton[4] and by Moore and his co-workers.[5] The chief differences between the dominant EPR spectra of NA and synthetic brown quartz (SBQ) are: a grossly unequal distribution of the $Fe^{3+}$ ions among the three sites in NA, a much greater zero-field splitting (24 and 35 GHz) in NA than in SBQ (7 and 9 GHz), and a different orientation of the crystal-field axes, i.e., while both centers share the three twofold crystallographic axes of quartz as one of the crystal-field axes of each site, the crystal-field axes in the planes perpendicular to the twofold axes are rotated by an angle of 57° from the optic axis of quartz in the case

[1] L. M. Matarrese, J. S. Wells, and R. L. Peterson, Bull. Am. Phys. Soc. 9, 502 (1964).

[2] A. R. Cook and L. M. Matarrese, J. Chem. Phys. 50, 2361 (1969), following paper.

[3] R. L. Peterson, L. M. Matarrese, and J. S. Wells, Natl. Bur. Std. (U.S.), Tech. Note 372 (1969).

[4] D. R. Hutton, Phys. Letters 12, 310 (1964).

[5] T. I. Barry and W. J. Moore, Science 144, 289 (1964). T. I. Barry, P. McNamara, and W. J. Moore, J. Chem. Phys. 42, 2599 (1965).

of NA and practically coincident with it in the case of SBQ. Lehmann and Moore[6] discuss the interrelation between these two centers as evidenced by optical absorption spectra and by heat and radiation treatments and conclude that the center in NA is substitutional ($S_1$), compensated by an interstitial alkali ion, and the center in SBQ is interstitial ($I$), perhaps compensated by a substitutional alkali ion. There is still room for doubt about this assignment, however, as will be seen in our discussion below.

Although the $S_1$ and $I$ centers are now the most thoroughly studied iron centers in quartz, their investigation represents only a small part of the problem of iron in quartz. The centers are only distantly related to the colors of NA and SBQ. The $S_1$ center, for example, is not directly responsible for the color of amethyst; the color can be produced by $x$ or $\gamma$ irradiation of quartz containing iron, with no trace of the $S_1$ spectrum appearing thereby.[6] Instead, another spectrum is found, due to an iron center labeled $S_2$, but even this is not the color center. A fourth spectrum has been described by Lehmann and Moore[7] that is presumably due to the color center itself, and which they identify as $Fe^{4+}$. We shall not delve into these matters here since it is our main purpose to give a more accurate and detailed description of the $I$ spectrum than has been available to date.

## II. EXPERIMENTAL OBSERVATIONS

### A. Crystallographic Conventions

Although quartz belongs to the trigonal system, point group 32, its crystal faces are commonly specified by means of the Bravais system, which is a four-axis hexagonal system in which the trigonal (optic) axis is called the $c$ axis, and the three twofold axes perpendicular to it are 120° apart and labeled $a_1$, $a_2$, $a_3$. Conventionally, the cyclical order of the subscripts 1, 2, 3 is counterclockwise when the axes are viewed from the positive end of the $c$ axis for both enantiomorphic forms of quartz. In quartz technology, it is conventional to use an orthogonal system $X$, $Y$, $Z$, with the $Z$ axis parallel to the $c$ axis, the $X$ axis parallel (antiparallel) to one of the $a$ axes in left (right) quartz, and the $Y$ axis perpendicular to the $X$ axis so as to form a left-handed (right-handed) coordinate system in left (right) quartz.[8] In our work, we have found it convenient to use this $X$, $Y$, $Z$ system. The handedness and the positive direction of the $X$ axis can be determined by simple optical tests and the study of etch figures.[9] A crystal of quartz is said to

[6] G. Lehmann and W. J. Moore, J. Chem. Phys. **44**, 1741 (1966). Additional data and discussion have just been published by G. Lehmann, Z. Naturforsch. **22a**, 2080 (1967). We thank the referee for bringing this to our attention.
[7] G. Lehmann and W. J. Moore, Science **152**, 1061 (1966).
[8] W. G. Cady, *Piezoelectricity* (McGraw-Hill Book Co., New York, 1946), Chap. 2.
[9] Reference 8, Chap. 16.

be right handed (dextrogyrate) if the direction of rotation of a beam of plane-polarized light passing through the crystal in the $Z$ direction appears to be clockwise to an observer looking back toward the source of light.

### B. Sample

In the EPR investigation, we examined specimens cut from three different samples of iron-doped synthetic quartz grown by the hydrothermal process by Sawyer. The solution in the autoclave was always $0.75M$ $K_2CO_3$. Crystals of $FeCl_2$ were added in the run that produced the first sample, E-23. The other two samples, D-51 and B-52, were grown from solutions to which crystals of $FeSO_4$ plus small amounts of sodium thiosulfate were added.

The synthetic crystals were in the form of $Y$ bars, i.e., they were grown on plate seeds, long in the $Y$ direction, with the $Z$ axis perpendicular to the plate. Growth on such a seed is fastest in the $\pm Z$ directions and progressively slower along $+X$, $-X$, $S$, minor $r$, major $r$, and $Y$, the last four directions being, respectively, perpendicular to the common natural faces of quartz conventionally labeled $s$ (trigonal bypyramidal), $z$ (minor rhombohedral), $r$ (major rhombohedral), and $m$ (hexagonal prismatic). The resulting $Y$ bar thereby has the appearance of an incompletely developed quartz crystal: the ends are terminated by well-developed $m$, $z$, and $r$ faces, but the lateral surfaces of the bar have a characteristic "cobblestone" texture on the surfaces perpendicular to $Z$ and a striated texture on the other surfaces.

Because of these differences in growth rates, it is natural to expect that there will be marked differences in the nature and amount of impurities taken up in the different growth regions. In general, the fastest growing regions are the purest. In the case of iron-doped quartz, the growth regions become visible by virtue of their differences in hue and intensity of the coloration produced by the iron, with rather sharp lines of demarcation between them. Examples of this are given in Fig. 1, which shows sketches of transverse sections of the D-51 and B-52 $Y$ bars. Sample E-23 had the same pattern of coloration as B-52, but the colors were much less intense.

Qualitative spectrographic analyses of samples taken from the $Z$-growth regions gave the following percentages of impurities: D-51, very-pale green portion near the seed; Fe, 0.01; Cu, 0.002; Al, B, Ca, Mg, Mn, Na, 0.001 each, Ag, Ti, 0.0001 each. D-51, green portion away from seed; Fe, 0.05; other elements same as above, except Cu and Mg, 0.005 each. B-52, brown portions; Fe, 0.07; B, Ca, Cu, Mg, Mn, Na, 0.001 each; Al, Cr, Ag, Ti, V, 0.0001 each. Sample E-23 was not analyzed; its Fe content in the $Z$-growth region was estimated to be about 0.02%.

The $Y$ bars were first cut into transverse sections to make $Y$ plates about 4 mm thick. The cross section

+X

YELLOW-GREEN

S

SEED

GREEN

Z

VERY PALE GREEN

YELLOW-GREEN

−X

(a) D-51

0    5    10

mm.

PALE GREEN

GREEN

SEED

BROWN
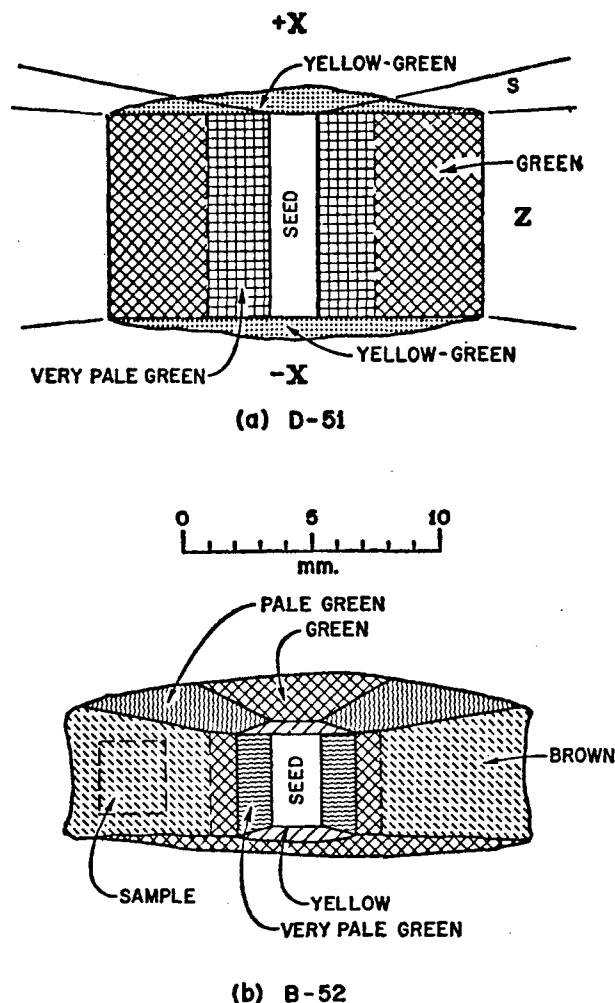
SAMPLE

YELLOW

VERY PALE GREEN

(b) B-52

Fig. 1. Transverse sections of $Y$ bars of synthetic iron-doped quartz.

of the seed plate was then clearly visible and was used as a reference for additional cuts. The final EPR specimens were approximate cubes, 4 mm on an edge, with the $X$, $Y$, and $Z$ directions known and essentially perpendicular to the cube faces. A simple experiment using crossed polaroids sufficed to check the position of the $Z$ axis and determine the handedness of the specimen. All of our specimens were found to be right handed. The specimen of B-52 used for the bulk of the EPR measurements was also etched in hydrofluoric acid in order to verify the positive direction of the $X$ axis by inspection of the etch figures.

## C. Spectrometer

Some of the preliminary work was done at $X$ band. The majority of measurements, however, were made at $K$ band. In both cases, the spectrometer was of the conventional bridge type with a reflection cavity and employed AFC on the sample cavity at 150 kHz, magnetic field modulation at 100 kHz, phase detection

at 100 kHz, and an $X$-$Y$ recorder with its $X$ axis synchronized with the magnetic field sweep.

The cavities were cylindrical $TE_{011}$ of the special thin-walled, band-and-groove design developed by us.[10] Coupling to the waveguide was effected through an iris in the top end-wall of the cavity and was adjusted by the motion of a Teflon slug in a section of cutoff waveguide immediately above the iris.[11] The samples were held in the center of the cavity by means of a Teflon sample holder passing through a central hole in the bottom of the cavity. This holder was essentially a ball-and-socket arrangement consisting of a flat disk (to which the sample was affixed with a tacky grease) above a ball on a thin rod that protruded through a Teflon socket in the bottom hole. This arrangement facilitated the precise alignment of the sample in the spectrometer by external adjustment of the rod.

The dc magnetic field was provided by a 12-in. electromagnet on a rotating base, the axis of rotation being vertical and parallel to the cavity axis. The field was measured to a precision of 0.1 G with a nuclear fluxmeter probe attached to a pole face near the cavity. No difference greater than the limits of precision was found between the field in the cavity at the sample position and the field at the probe.

## D. Spectra

All EPR measurements reported here were made with the sample at room temperature.

Our first observations were made on a specimen cut from E-23. Both brown and green portions gave the same spectrum: A well-behaved five-line spectrum centered at $g=2$ from each of three equivalent, but differently oriented sites, together with many lines which resembled the amethyst spectrum.[5] The lines from both groups were quite narrow, averaging 5 G between inflection points. In addition, at $X$ band there was a broad (375-G) line of comparable signal height whose position remained near $g=2$ for all orientations. This line was not in evidence in the $K$-band runs.

Samples cut from the $Z$-growth region of D-51 gave the same results.

Both E-23 and D-51 could be bleached by heat treatment at 600° C. Although the samples became almost colorless, the EPR spectra were essentially unchanged. Besides losing their color, the samples also became milky.

The spectrum of a sample taken from the brown $Z$-growth region of B-52 (see Fig. 1) differed in one important respect from those just described: it consisted almost exclusively of the well-behaved five-line spectrum. Although other lines were occasionally observed, their intensities were negligible. Since the five-line spectrum could now be studied without

[10] A. R. Cook, L. M. Matarrese, and J. S. Wells, Rev. Sci. Instr. 35, 114 (1964).

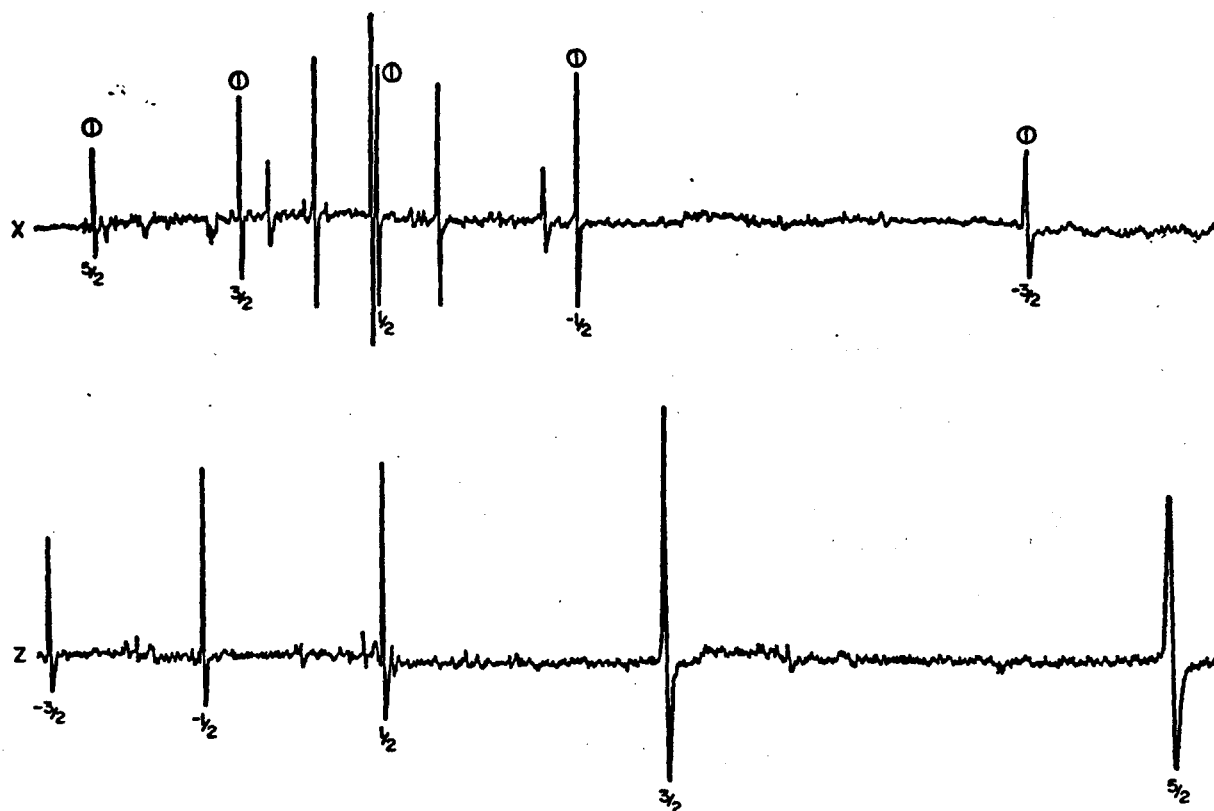[11] J. P. Gordon, Rev. Sci. Instr. 32, 658 (1961).

FIG. 2. Representative EPR spectra of $Fe^{3+}$ in SBQ along $X$ and $Z$. In the upper trace, the circled numbers indicate the lines from site 1, the site whose principal axis lies along this particular $X$ direction. The other two sites are equivalent here. In the lower trace all three sites are equivalent.

interference from other lines, it was decided to concentrate on this sample, and all further results given here pertain to it alone.

The intensities of the five lines were very roughly in the ratios 5:8:9:8:5, with the strong central line always near $g=2$. This pattern is typical of a ferric ion in a predominantly axial field. When the magnetic field was along the $Z$ axis, a single set of five lines was observed. When the magnetic field was rotated in a plane perpendicular to the $Z$ axis, the spectrum in general consisted of three equally intense sets of five lines and repeated itself accurately every 60°. But whenever the field was along one of the twofold axes ($a_1$, $a_2$, $a_3$), the spectrum degenerated into two sets of five lines, one set being twice as intense as the other. Figure 2 shows the appearance of the spectra along $X$ (a twofold axis) and $Z$.

These facts clearly indicate that the three sites are equivalent and are located on the twofold axes. Unlike the situation in amethyst,[5] the sites were nearly equally populated in our specimen.

The lines were narrowest with the field along $X$, the central component having a width of 2.4 G, the inner satellites 3.2 G, and the outer satellites 4.8 G. Along $Z$ or $Y$ these widths were 2.7, 4.0, and 6.0 G, respectively.

The angular dependence of the spectrum was investigated in three separate rotations about the $X$, $Y$, and $Z$ axes. Line positions were measured every 15°. The results are shown in Figs. 3–5, respectively. Full use was made of the symmetry properties of the three sites in the alignment of the specimen for these studies. An iterative procedure involving rotations of the magnet and manipulations of the sample holder in two perpendicular planes was used. For the rotations about $X$ and $Y$, the criterion for best alignment was the best simultaneous superposition of the spectra from all three sites for $H \parallel Z$, and from two of them when the magnet was rotated exactly 90°, making $H \parallel Y$ for the rotation about $X$ and $H \parallel X$ for the rotation about $Y$. A further check in the rotation about $X$ was that the spectra from two of the sites should be superposed at all angles. The fact that this is not true for rotation about $Y$ has certain implications that will be discussed in the theory section.

For the rotation about $Z$, the sample was adjusted until the spectra from two sites superposed every 60°. An indication of the perfection of alignment in this case is that when the line positions at 0° ($H \parallel X$) and ±60° were measured, they were found to agree to within a few tenths of a gauss, which is considerably less than the linewidth.
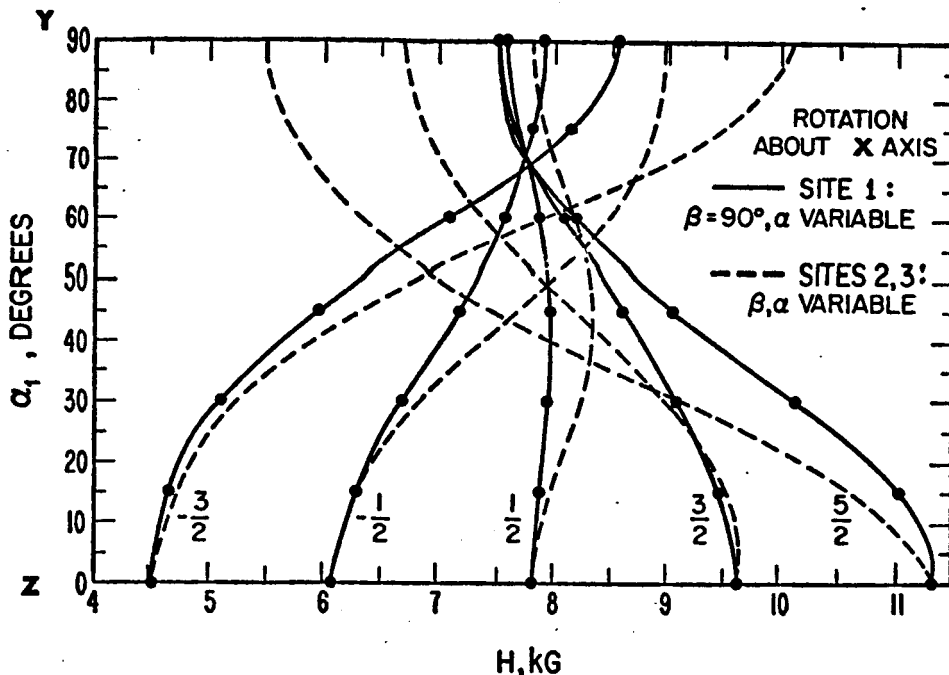
FIG. 3. Angular dependence of the EPR spectrum of SBQ, rotation about an $X$ (twofold) axis of quartz. See text for definitions of angles. Points are experimental; lines are theoretical.

It may appear from the figures that the magnetic axes for site 1, say, are the $X$, $Y$, $Z$ axes themselves, since the lines appear to have extremal positions in those directions. More careful work in the vicinity of these directions, however, discloses that all five lines do indeed have extrema in the $X$ direction, but in the vicinity of $Y$ and $Z$ the different lines have extrema at different places, varying from $+1.5°$ to $-8°$ from the $Y$ axis and $+1.0°$ to $-3.5°$ from the $Z$ axis. (See Figs. 6 and 7) The explanation of this

is given in the theory section. Associated with this phenomenon is the fact that when $\mathbf{H}$ is in the $YZ$ plane, the spectrum for site 1 is not symmetrical with respect to the $Z$ axis. Figure 3 shows only one quadrant in this plane; the other quadrant is different. The quadrants on both sides of the $Z$ axis in the $XZ$ plane have identical appearances, but actually the lines from sites 2 and 3 change places, i.e., a line from site 2 at a given position in one quadrant corresponds to a line from site 3 at the same position in
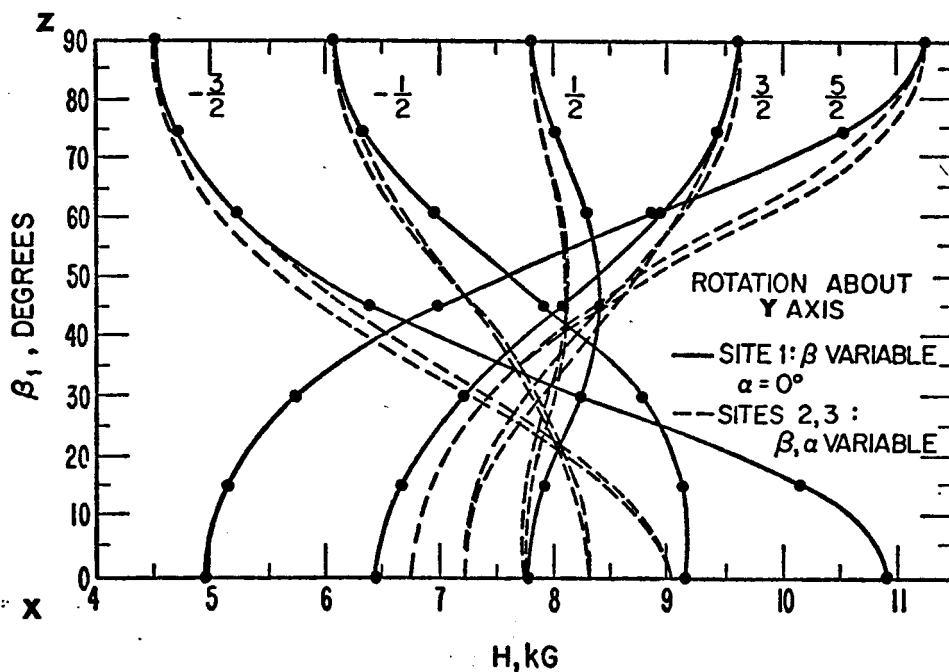


FIG. 4. Angular dependence of the EPR spectrum of SBQ, rotation about the $Y$ axis of quartz. See text for definitions of angles. Points are experimental; lines are theoretical.

ROTATION ABOUT **Z** AXIS

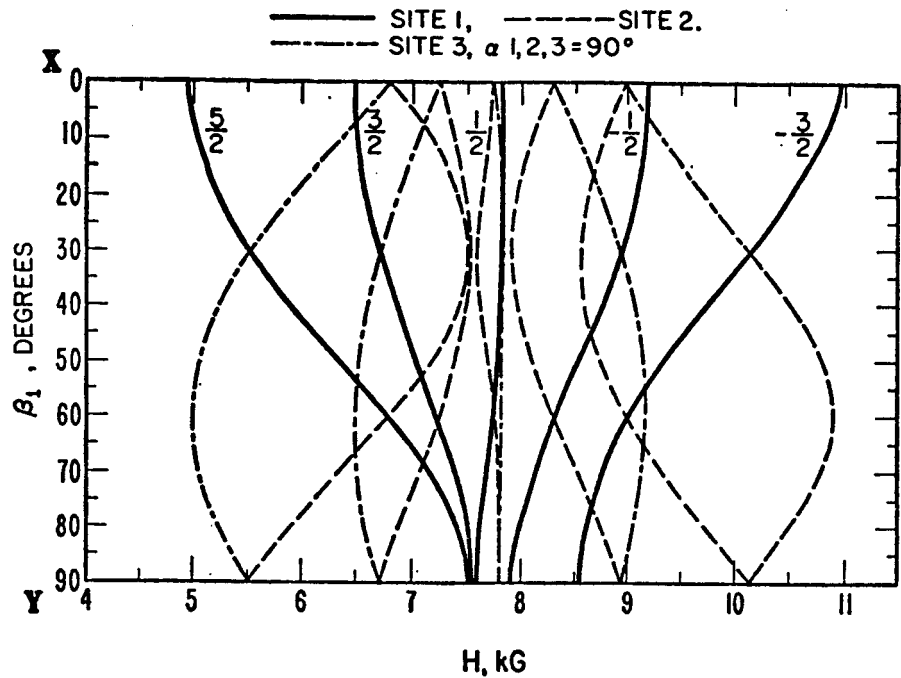——— SITE I,  ———— SITE 2.
——·——·— SITE 3,  $a\ 1,2,3=90°$

FIG. 5. Angular dependence of the EPR spectrum of SBQ, rotation about the $Z$ (optic) axis of quartz. See text for definitions of angles. The lines are drawn through the experimental points, which are omitted here for greater clarity.
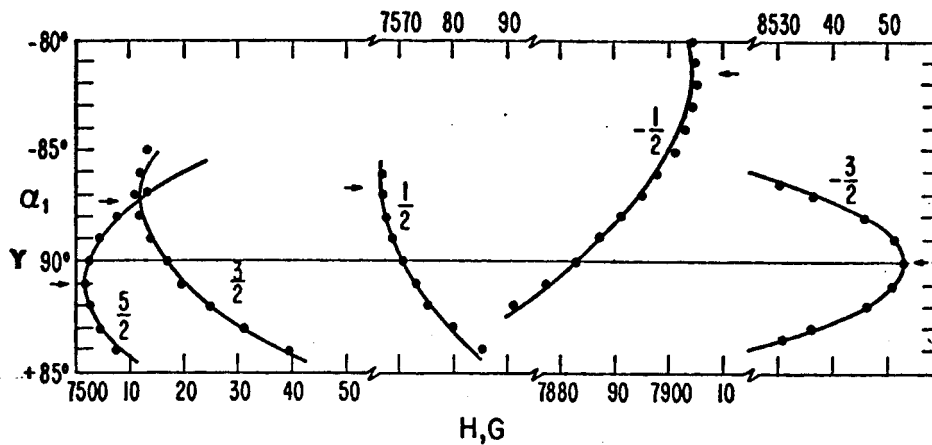
ROTATION ABOUT **X**: OFF–AXIS EXTREMA NEAR **Y**

FIG. 6. Off-axis extrema of the Fe³⁺ spectrum in SBQ (site 1) in the $YZ$ plane, near the $Y$ axis. Points are experimental; lines are theoretical.

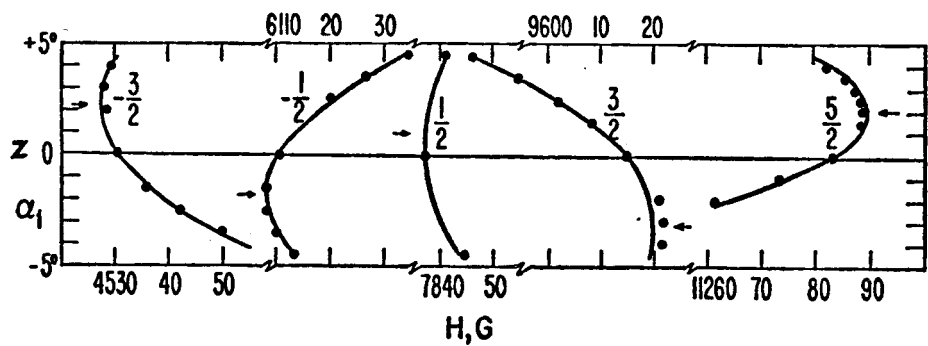ROTATION ABOUT **X** : OFF–AXIS EXTREMA NEAR **Z**

FIG. 7. Off-axis extrema of the Fe³⁺ spectrum in SBQ (site 1) in the $YZ$ plane, near the $Z$ axis. Points are experimental; lines are theoretical.
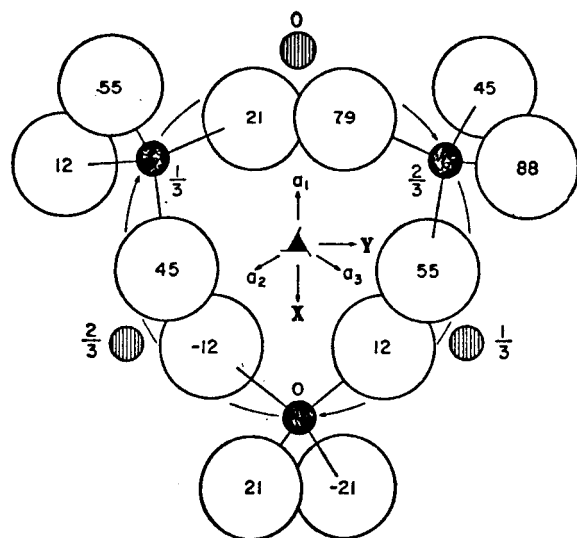
FIG. 8. Positions of Si (small circles) and O (large circles) in right-handed quartz, view along the $Z$ axis. The numbers beside the Si indicate height above the basal plane as fractions of the lattice parameter $c_0$ in this direction. The numbers inside the O circles give the height in hundredths of $c_0$. The solid Si circles are related by the threefold screw axis parallel to $Z$. The circles are to half-scale for clarity.

the other quadrant. In the $XY$ plane, the same situation obtains with respect to the $X$ axis.

Further experimental work included a series of experiments to determine whether discrepancies between calculated and observed line positions at intermediate angles could be attributed to misalignment of the crystal. It was found in rotation about $X$, for example, that any misalignment sufficient to cause a detectable splitting of the lines from sites 2 and 3 did not appreciably change the positions of the lines from site 1. Such misalignments would have been eliminated, of course, in the alignment procedure.

Another experiment was designed to detect the presence of a spherical harmonic $Y_{21}$ term in the spin Hamiltonian, with negative results. This is described more fully in the theory section.

Preliminary low-temperature work with the sample temperature below $2°$ K disclosed that when $H$ was parallel to the $X$ axis, which was chosen as the principal axis of the crystal field, the high-field transitions were relatively much more intense than at room temperature. This implies that the sign of $D$, the second-degree axial field parameter, is positive.

## III. THEORY

The experimental results show conclusively that the $Fe^{3+}$ ions are in three differently oriented but otherwise equivalent sites. Each site has a principal axis that is parallel to one of the $a$ axes, of which there are three, $120°$ apart in a plane perpendicular to the $c$ ($Z$) axis. The other axes must have the same orientation with respect to the $c$ axis for all three sites since all three sites give identical spectra when $H \parallel c$.

Right-handed quartz belongs to the space group $P3_221(D_3^6)$.[12] Figures 8 and 9 show the positions of the silicon and oxygen atoms in the quartz structure, a unit of which can be visualized as a set of three $SiO_4$ tetrahedra that are carried into each other by the operation of the left-handed threefold screw axis of the space group shown in the figure. The silicon sites are on a set of similarly related twofold axes and are therefore possible sites for the ferric ions. As is well known, quartz has relatively open channels parallel to the $c$ and $a$ axes; these can easily be seen in the figures. Not readily apparent in the figures are other channels intersecting the first two and making an angle of about $57°$ with the $c$ axis. It has been known for a long time that small positive ions diffuse readily through the quartz channels. Therefore, the possibility that the ferric ions are on interstitial sites in these channels must also be considered. There are two such interstitial sites on twofold axes. One, which we shall call $I_c$, is in the $c$-axis channel, at or near the intersection of the threefold screw axis shown in Fig. 8, and the twofold axis joining equivalent Si sites. The other, $I_a$, is in the $a$-axis channel, halfway between two equivalent Si sites in the $c$ direction.

It turns out that the point-group symmetry at any of these sites is $2(C_2)$. Moreover, the sets of twofold axes for the $S$ (substitutional) and $I_c$ sites are identical to each other and parallel to the set for $I_a$. Barring
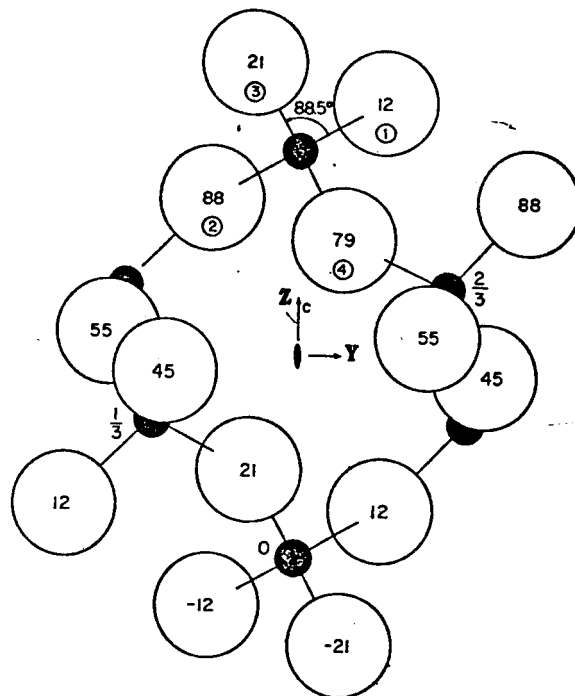


FIG. 9. Positions of Si (small circles) and O (large circles) in right-handed quartz, view into the positive end of an $X$ axis. The numbers indicate height above the basal plane in the $Z$ direction, and the circles are to half-scale, as in Fig. 8.

[12] A. DeVries, Nature 181, 1193 (1958).

any distortions arising from the introduction of foreign ions which would affect the symmetry of the spin Hamiltonian, therefore, the assignment of the ferric ion to a given type of site cannot be decided from this symmetry alone. Leaving this question for the discussion section, we shall go on with an explanation of how we fit a spin Hamiltonian to the EPR data.

Since the three $Fe^{3+}$ sites differ only in the orientation of their twofold axes in the basal plane, we shall restrict our attention to the data for site 1, i.e., the site whose twofold axis is parallel to $X$. This axis is unique not only as the sole symmetry axis of the group $C_2$, but also as the only direction in which all site 1 lines have extrema. We therefore choose it as the polar $(r)$ axis of the $(p, q, r)$ orthogonal coordinate system of the crystal field. It should be remarked that the usual convention of minimizing the $E/D$ ratio leads to the choice of the $Z$ direction as the $r$ axis for the $I$ center.[6] It would be awkward to apply this convention in our case in view of the nature of our crystal-field Hamiltonian.

The crystalline electric field potential appropriate for $Fe^{3+}$ in surroundings of $C_2$ symmetry contains only the following terms:

$$V = V_{20} + V_{22} + V_{40} + V_{42} + V_{44}, \qquad (1)$$

where

$$V_{lm} \equiv a_{lm} Y_{lm} + a_{lm}{}^* Y_{lm}{}^*. \qquad (2)$$

The $Y_{lm}$ can be written

$$Y_{lm} = f_{lm}(\theta) \exp(im\phi), \qquad (3)$$

where $f_{lm}(\theta)$ is real, $\theta$ is the polar angle of a volume element from the $r$ axis, and $\phi$ is the azimuthal angle in the $pq$ plane, measured from the $p$ axis. Thus if we put

$$a_{lm} = b_{lm} \exp(-im\lambda_{lm}), \qquad (4)$$

with $b_{lm}$ and $\lambda_{lm}$ real and $b_{lm} > 0$, we see that $V_{lm}$ is proportional to $\cos m(\phi - \lambda_{lm})$.

We remark parenthetically that if only the nearest-neighbor oxygen atoms are considered, the $S$ and $I_c$ sites almost have $C_{2v}$ symmetry, i.e., the dihedral angle between the $O_1$–$Si$–$O_2$ and $O_3$–$Si$–$O_4$ planes is only 1.5° different from 90°. (See Fig. 9.) This higher symmetry would require the $a_{lm}$ for $m \neq 0$ to be real. (The coefficients $a_{20}$ and $a_{40}$ are obviously real.) In simple cases, e.g., when the potential (1) consists only of the first three terms, or when $\lambda_{22} = \lambda_{42} = \lambda_{44}$, $a_{22}$ can be made real in the $C_2$ case as well by a proper choice of the $p$ and $q$ axes so that they lie along the lobes of $V_{22}$. Since at an extremum of a $V_{lm}$ lobe $|\cos m(\phi - \lambda_{lm})|$ is unity, we see that $\lambda_{22}$ is the angle of a $V_{22}$ lobe extremum from the $p$ axis, and the $p$ axis can be chosen so that this angle is zero. All the lines of the EPR spectrum can then be expected to have extrema when $H \parallel p$.

This device could not be used in our case since the irregularity of the off-axis extrema and analysis of
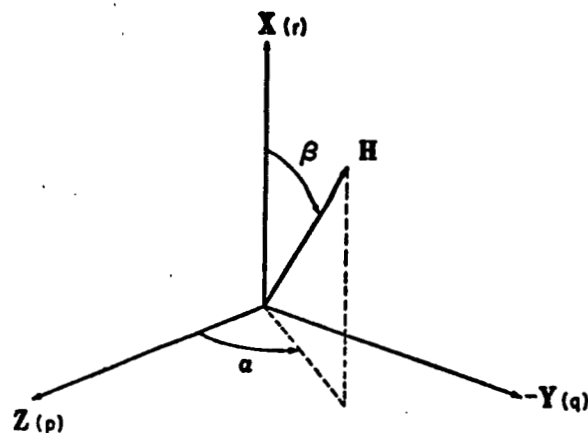


FIG. 10. Coordinates used in the analysis.

the data indicate that $V_{44}$ is important and $\lambda_{44}$ is different from $\lambda_{22}$. We could therefore orient $p$ along the $Z$ axis since the latter lies in the $pq$ plane, or we could orient $p$ along one of the lobes of either $V_{22}$ or $V_{44}$, which would have the effect of making either $\lambda_{22}$ or $\lambda_{44}$ zero, but not both. We made the former choice and set $p \parallel Z$.

In developing the spin Hamiltonian, we used the technique of Kikuchi and Matarrese,[13] in which the $Y_{lm}$ are replaced by the Racah operators $T_m{}^{(l)}$. Analysis of the experimental data showed that the $g$ tensor was essentially isotropic. Thus we write for the spin Hamiltonian

$$\mathcal{K} = g\beta_0 \mathbf{H} \cdot \mathbf{S} + C_{20} T_0{}^{(2)}$$
$$+ C_{22}[T_2{}^{(2)} \exp(-2i\lambda_{22}) + T_{-2}{}^{(2)} \exp(2i\lambda_{22})] + C_{40} T_0{}^{(4)}$$
$$+ C_{42}[T_2{}^{(4)} \exp(-2i\lambda_{42}) + T_{-2}{}^{(4)} \exp(2i\lambda_{42})]$$
$$+ C_{44}[T_4{}^{(4)} \exp(-4i\lambda_{44}) + T_{-4}{}^{(4)} \exp(4i\lambda_{44})], \quad (5)$$

where all $C_{lm}$ are real. The signs of $C_{20}$ and $C_{40}$ must be determined by experiment, which showed both to be positive. The signs of the other $C_{lm}$ are arbitrary and were chosen to be positive. The $T_m{}^{(l)}$ of Eq. (5) have been normalized so as to make $C_{20}$ identical to the common axial-field parameter $D$. Also $C_{22} = (6^{1/2}/2)|E|$.[14]

To use perturbation theory it is convenient to diagonalize the first term of (5) by rotating (5) from the crystal-field coordinate system $(p, q, r)$ to the magnetic-field coordinate system $(x, y, z)$, where $z$, the axis of quantization, lies in the direction of $\mathbf{H}$. This results in the introduction of two angles, $\alpha$ and $\beta$, which define the direction of $\mathbf{H}$ relative to the quartz crystallographic axes (Fig. 10). The matrix elements

[13] C. Kikuchi and L. M. Matarrese, J. Chem. Phys. **33**, 601 (1960).

[14] Unfortunately, there is really no standard notation for spin Hamiltonians when it is inappropriate, as in this case, to divide the field into axial, rhombic, and cubic components. The notation of Eq. (6) is logical and natural and divides the field into readily understood $Y_{lm}$ components. We feel the consistent use of such a notation in all EPR work would be very desirable.

TABLE I. Values of the spin-Hamiltonian parameters for $Fe^{3+}$ in SBQ.

| Parameter | Value[a] | | |
|---|---|---|---|
| | Initial | Final | |
| $g$ | 2.0040 | $2.0039 \pm 0.0001$ | |
| $\lambda_{22}$ | 91.0° | $90.70 \pm 0.02°$ | |
| $\lambda_{42}$ | ... | $29.5 \pm 4.5°$ | |
| $\lambda_{44}$ | 71.5° | $71.8 \pm 0.3°$ | |
| | (MHz) | (MHz) | (G) |
| $C_{20}$ | 2061.0 | $2059.6 \pm 0.9$ | $734.3 \pm 0.3$ |
| $C_{22}$ | 1127.8 | $1126.6 \pm 0.6$ | $401.7 \pm 0.2$ |
| $C_{40}$ | 6.90 | $7.06 \pm 0.12$ | $2.52 \pm 0.04$ |
| $C_{42}$ | ... | $0.58 \pm 0.12$ | $0.21 \pm 0.04$ |
| $C_{44}$ | 4.60 | $3.91 \pm 0.11$ | $1.40 \pm 0.04$ |

[a] The error limits shown are estimates of the standard deviation as provided by computer program PARA.

of (5), a description of the modified perturbation treatment we used, and the resulting line-position formulas are given elsewhere.[3]

We used these formulas to obtain good estimates of the spin-Hamiltonian parameters, using the data for $H \parallel X, Y, Z$ (15 lines). These were then used as initial values in a computer diagonalization program called PARA[15] to produce a least-squares fit to 35 observed line positions ($H \parallel X, Y, Z$, and four other directions). Table I gives the initial and final parameter values. One sees that the perturbation results are changed only slightly; the main effect of the computer program was to improve the fit of line positions throughout the entire range of angles. With the perturbation treatment, the precision of the fit along $X$, $Y$, and $Z$ was better than 0.1%, but worsened to a maximum discrepancy of 1.6% in the rotation about $X$ and 3.4% about $Y$. With the computer program, the maximum discrepancy at any angle was less than 0.1%. The curves in Figs. 3 and 4 are drawn through the line positions calculated by the computer.

All of the characteristic features of the three rotations can be understood on the basis of our spin Hamiltonian; the splitting of sites 2 and 3 in the rotation about $Y$, as well as the off-axis extrema in the rotation about $X$ (Figs. 6 and 7), is well described by it. The following relations among the sites can be deduced from their presumed orientation in the lattice (the $p$ axes of all three sites parallel to $c$, their $r$ axes, respectively, parallel to the $a$ axes):

$$\cos\beta_{2,3} = \pm\tfrac{1}{2}\sqrt{3} \sin\beta_1 \sin\alpha_1 - \tfrac{1}{2} \cos\beta_1, \quad (6)$$

$$\sqrt{3} \sin\alpha_{2,3} = \pm 2(\cos\beta_1/\sin\beta_{2,3}) \pm \operatorname{ctn}\beta_{2,3}, \quad (7)$$

[15] H. M. Gladney, Phys. Rev. 143, 198 (1966).

where the upper signs are for site 2. For the special cases of the $X$, $Y$, and $Z$ rotations we have the formulas of Table II.

In the line-position formulas[3] $\cos\beta$ appears only in even powers. Therefore sites 2 and 3 are equivalent in the rotation about $X$. The absence of splitting is also a contraindication for a $V_{21}$ term since the angular dependence of this term, to first order, is $\sin\beta\cos\beta \cos(\alpha-\lambda_{21})$. From the first-order angular dependence of $V_{22}$, $\sin^2\beta\cos2(\alpha-90.7°)$, it is seen that all the site-1 lines should have extrema 0.7° away from the $Z$ axis. If it were not for the presence of $V_{44}$, this direction could be chosen as the $p$ axis. The effect of $V_{44}$ is to mix up the extrema in such a way that no such well-defined direction can be chosen. The most that can be said is that the lobes of $V_{22}$ and $V_{42}$ point 0.7° and 29.5° from the $Z$ axis (and every 90° from there), and the $V_{44}$ lobes point 26.8° from $Z$ (and every 45° from there).

The splitting of sites 2 and 3 in the rotation about $Y$ is due to the fact that $\alpha_2 = -\alpha_3$. From the line-position formulas[3] it can be seen that the splitting in first order is then proportional to $C_{22}\sin2\alpha_2\sin2\lambda_{22}$. A $V_{21}$ term would also give a splitting, which, however, would be difficult to disentangle from the $V_{22}$ contribution.

In the rotation about $Z$, sites 2 and 3 are equivalent when $\beta_1 = 0$, 90°, sites 1 and 3 at $\beta_1 = 30°$, and sites 1 and 2 at $\beta_1 = 60°$. It is interesting to note that this would not be true if a $V_{21}$ term were present, unless $\lambda_{21} = 0$.

Since it was possible that our alignment procedure may have operated to hide the presence of a small $V_{21}$ term, we performed a special experiment designed to detect it. Briefly, this consisted of so mounting the crystal that a 90° rotation of the magnet would change $\alpha_1$ to $\alpha_1 + 180°$, while $\beta_1$ would have the same value (45°) for both positions. If $V_{21}$ is present there should be a shift in a given line position proportional to $C_{21}\cos(\alpha_1-\lambda_{21})$. There was no deviation from coincidence of the two spectra greater than that attributable to error in positioning the magnet (about 0.1°).

For $H \parallel X$, the matrix of the Hamiltonian simplifies

TABLE II. Relations among the angles for the $I$ sites in SBQ.

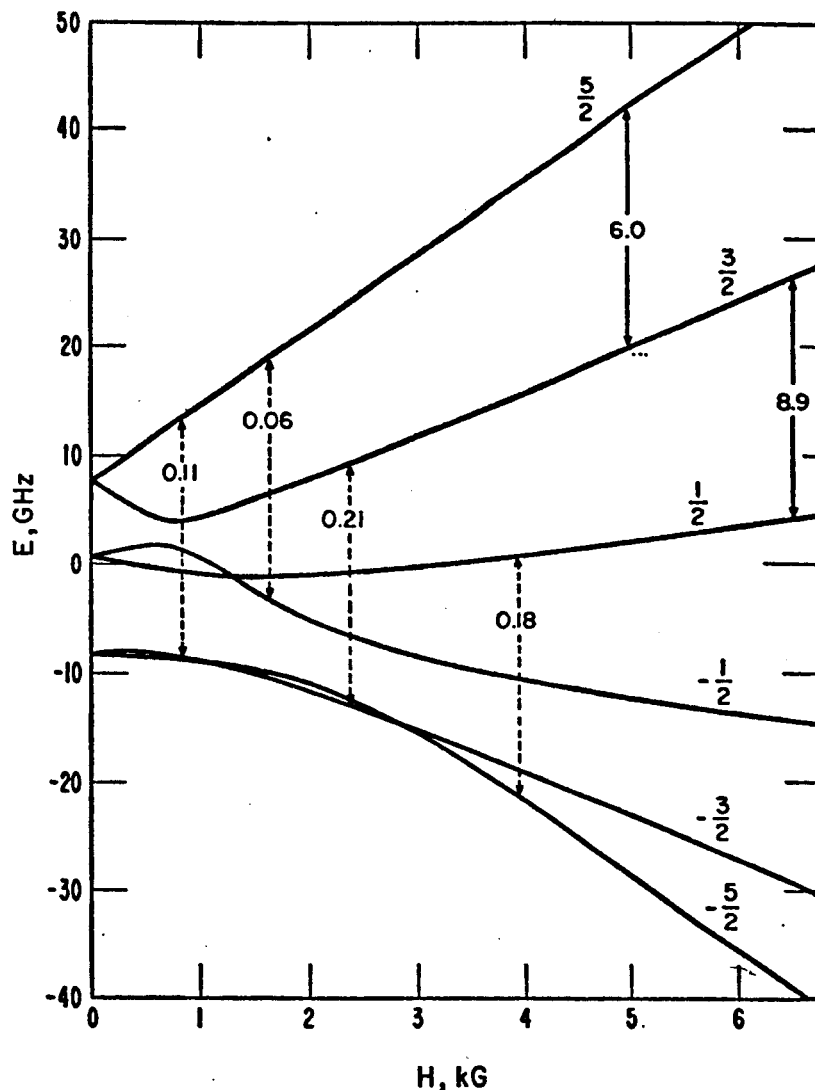| Site | Rotation about | | |
|---|---|---|---|
| | $X$ | $Y$ | $Z$ |
| 1 | $\alpha_1$ variable | $\alpha_1 = 0°$ | $\alpha_1 = -90°$ |
| | $\beta_1 = 90°$ | $\beta_1$ variable | $\beta_1$ variable |
| 2, 3 | $\alpha_2 = \alpha_3$ | $\alpha_2 = -\alpha_3$ | $\alpha_2 = 90°$ |
| | $\beta_2 = 180 - \beta_3$ | $\beta_2 = \beta_3$ | $\alpha_3 = -90°, +90°$ |
| | $\cos\beta_{2,3}$ | $\cos\beta_{2,3}$ | $\beta_{2,3} = 120° \mp \beta_1$ |
| | $= \mp \tfrac{1}{2}\sqrt{3}\sin\alpha_1$ | $= -\tfrac{1}{2}\cos\beta_1$ | |

FIG. 11. Calculated energy-level diagram for Fe$^{3+}$ in SBQ, with the field along the principal axis of a site. Solid arrows show two of the $\Delta M = 1$ transitions. Dashed arrows show $\Delta M = 3$ and $\Delta M = 5$ transitions. The numbers on the arrows are the relative transition probabilities for the rf field perpendicular to H.

to the extent that the energy-level formulas can be derived analytically.[3] The initial parameters of Table I were used to calculate the energy levels from such formulas, as a function of $H$, by computer. These are shown in Fig. 11. The positions of the $\Delta M = 1$ transitions, of which only the two lowest are indicated in the figure, agree with the observed line positions to better than 0.03%. Of the three $\Delta M = 3$ transitions indicated, the upper two were observed within 50 G of their calculated positions with a signal-to-noise ratio of about 2. The lowest of the $\Delta M = 3$ transitions and the $\Delta M = 5$ transition were not found; they could well have been hidden in the noise. The zero-field splittings calculated from the final parameter values are 7109.8 and 8775.6 MHz.

## IV. DISCUSSION

The Hamiltonian which best fits the $I$ spectrum demands that the Fe$^{3+}$ be in a site of twofold symmetry with its principal axis along $X$. Any one of the three sites $S$, $I_a$, $I_c$, either with a local compensator on the principal axis or without one, could therefore be logically chosen as the location of the $I$ center. On the other hand, the $I_a$ site with a substitutional compensator in the $Z$ direction appears to be ruled out; it seems that such a structure would have sufficient distortion to add a $V_{21}$ term, which we did not find.

Lehmann and Moore[6] assigned the $I$ center to an interstitial site by interpreting the differences in the optical absorption spectra of NA and SBQ to mean that the Fe$^{3+}$ ion in SBQ is in one of the roomier interstitial sites. They also argued that the much larger zero-field splitting of the $S_1$ center implies that this center is in the more constricted substitutional site, where the crystalline field is presumably greater. However, by expanding the Coulomb field at this site in spherical harmonics,[13] we have found that the polar angles of the ligand ions are far more important than

their distances from the center in determining the magnitude of, say, $a_{20}$, the second-degree axial contribution. The four oxygens at the site $S$ are very nearly on the vertices of a regular tetrahedron, for which $a_{20}$ vanishes when a twofold axis is chosen as the principal axis. In fact, the value of $a_{20}$ can be made to vary over an extremely wide range merely by allowing for the errors in the parameters that locate the atoms in the quartz structure.[16,17] We therefore feel that a substitutional site for the $I$ center cannot be ruled out on the basis of the size of the spin-Hamiltonian parameters.

From the field calculation referred to above, we obtained values of $\lambda_{22}$, $\lambda_{44}$, and $R \equiv (a_{22}/a_{20})^2$ (assumed to be a rough measure of $C_{22}/C_{20}$). For the undistorted $S$ site without local charge compensation, we obtained, taking into account only the four nearest oxygens (1, 2, 3, 4 in Fig. 9), $R=33.7$, $\lambda_{22}=-29°$, $\lambda_{44}=28.6°$. When the four nearest silicons were added, we found $R=0.19$, $\lambda_{22}=0.5°$, $\lambda_{44}=27.1°$. These may be compared with our experimental values $C_{22}/C_{20}=0.55$, $\lambda_{22}=0.7°$, $\lambda_{44}=26.8°$ for the $I$ spectrum. The large change when just four more charges are added suggests that this better agreement is fortuitous. When a unit positive charge is added in the $c$-axis channel midway between two $S$ sites, $\lambda_{22}$ and $\lambda_{44}$ remain the same, but the axial contribution $(a_{20})$ is actually decreased—we find $R=0.78$ and is quite sensitive to the precise distance of the charge from the $S$ site under consideration. Similar calculations on the interstitial sites gave results more in keeping with the parameters of the $S_1$ spectrum. It is clear, however, that this approach cannot lead to conclusive results unless one is willing to compute more complete lattice sums for all the possible configurations and distortions that appear reasonable.

The broad isotropic line at $g=2$ is believed[6] to be due to precipitated $Fe_2O_3$ and peculiar to natural crystals of amethyst and citrine. However, as mentioned above, we have observed it in synthetic crystals.

## V. CONCLUSION

The results reported here, while giving a more precise EPR picture of the $Fe^{3+}$ center in quartz called $I$, do not settle the question of whether or not the site is actually interstitial. Notwithstanding the optical evidence cited by Lehmann and Moore,[6] we believe the data are more easily understood if the $I$ center is assigned to a substitutional site and that the difference between $I$ and $S_1$ is only a difference in location or type of compensator, which is probably an alkali ion. It is clear that other types of evidence are needed to solve this problem: One can look for off-axis extrema and a $V_{21}$ term in the Hamiltonian for the $S_1$ center. Electrolysis experiments can be tried, where one attempts to move the $Fe^{3+}$ ions about in the crystal under the influence of electric fields applied in specific directions at elevated temperatures. We have in mind investigating the EPR spectrum while the crystal is being heated to temperatures near the transition of quartz to high-quartz. Here there is a change in the $c_0/a_0$ ratio and also a change of crystal symmetry. Although there is no evidence of hyperfine structure (except in one line of the $S_1$ spectrum[5]) and the lines are narrow, some ENDOR experiments could be tried to detect a possible interaction with alkali ions. Such investigations may furnish additional clues to the configurations of the iron centers in quartz.

[16] H. D. Keith, Proc. Phys. Soc. (London) B63, 208, 1034 (1950).
[17] R. Brill, C. Hermann, and C. Peters, Ann. Phys. 41, 233 (1942).